Room-temperature operation of a nanoelectromechanical resonator embedded in a phase-locked loop

T. Kouh, O. Basarir, and K. L. Ekinci[a)]
Aerospace and Mechanical Engineering Department, Boston University, Boston, Massachusetts 02215

(Received 30 March 2005; accepted 22 July 2005; published online 9 September 2005)

We describe the operation of a phase-locked loop (PLL) that tracks the high-frequency electromechanical resonance of a nanoscale beam resonator. The fundamental in-plane flexural resonance of the beam resonator embedded in the PLL is actuated electrostatically and detected optically. PLL operation is demonstrated by locking stably to the resonance frequency of the beam, and by tracking this resonance with high fidelity as the beam is mass loaded. Our analysis reproduces the observed locking behavior. Feedback control schemes for nanoelectromechanical resonators may offer prospects for miniature timekeeping devices and ultrasensitive sensors. © *2005 American Institute of Physics*. [DOI: 10.1063/1.2048813]

Microelectromechanical systems (MEMS) are rapidly being miniaturized[1] following the trend in commercial transistor electronics. The emerging nanoelectromechanical systems (NEMS) possess high resonance frequencies, high quality (Q) factors and minuscule active masses, and present unique technological opportunities—especially in sensing[2] and timekeeping[3] applications. In resonant mass sensing, for instance, a feedback circuit tracks the resonance frequency of the sensor element and thus provides a frequency shift that is directly proportional to the inertial mass accreted upon the sensor.[2] In this realm, unprecedented NEMS mass sensitivities could ultimately allow weighing individual molecules.[4] In timekeeping, one usually references the resonance frequency of a high Q electromechanical resonator, such as a quartz crystal, in an oscillator circuit.[5] Here, NEMS with on-chip control electronics could obviate the need for externally packaged frequency reference elements.[6] To achieve the full potential of NEMS in both applications, it is necessary to develop low noise frequency control schemes for NEMS operating at room temperature.

In this letter, we describe the *room-temperature* operation of a NEMS resonator embedded in a phase-locked loop (PLL). The PLL approach[2,7] achieves the same end result as a self-driven resonator[8] without the need for thermomechanically limited displacement detection. The work presented here has several other interesting facets in addition to the PLL design, operation, and analysis. First, the NEMS resonator employed has a unique geometry. It is fabricated on a membrane and is accessible from both the top and the bottom sides: by an optical probe from the top, and by a molecular beam from the bottom. Second, detection of in-plane NEMS motion is demonstrated using simple optical reflection. Most optical displacement measurements on NEMS up to date have been sensitive to *out-of-plane* NEMS motion.[9]

The NEMS resonators used in these experiments were silicon nitride doubly clamped beams. A representative structure is shown in the upper inset of Fig. 1. The electrically isolated side gate is for in-plane capacitive actuation. The devices were fabricated on a silicon wafer with 125-nm-thick silicon nitride coatings on both sides. The first step in our device fabrication was the preparation of a silicon nitride membrane. The beam-gate structure was patterned on the membrane using electron beam lithography, thermal mask deposition, lift-off, and reactive ion etching.

The silicon nitride doubly clamped beam resonator was operated at room temperature inside an ultrahigh vacuum (UHV) chamber. This chamber allowed optical device probing through a quartz viewport. In addition, through the backside opening on the chip, we could thermally evaporate Au atoms upon the beam resonator to change its effective mass. In the experiments, the motion of the beam was actuated capacitively through the side gate. To detect the resulting in-plane motion, we implemented a simple optical reflection measurement. For this, a He–Ne laser was focused upon the device into an optical spot size of 1.2 μm and the intensity of the light reflecting from the device was monitored by a photodetector. In the measurements, we found out that if the optical spot was carefully positioned on the nanomechanical beam, the motion of the highly reflective metallized beam modulated the reflected optical power, and hence, the photodetector current I. Figure 1 shows the in-plane fundamental flexural resonance of a $14\ \mu\mathrm{m} \times 200\ \mathrm{nm} \times 125\ \mathrm{nm}$ ($l \times w \times t$) doubly clamped beam with a 100-nm-thick aluminum metallization layer, as measured by the optical reflection technique. The lower inset in the figure displays the displacement responsivity $\partial I / \partial x$ of the technique as a function of the optical spot position on the structure. Here, the optical spot was scanned across the structure along the x axis. In the

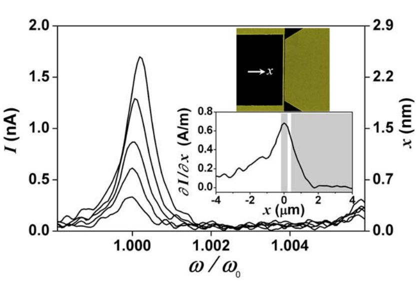

FIG. 1. (Color online) In-plane fundamental flexural resonance of a beam (upper inset) with $l = 14\ \mu$m, $w = 200$ nm, and $t = 125$ nm at $\omega_o / 2\pi \approx 7.9440$ MHz for increasing drive amplitudes as measured by the optical reflection technique. The gap between the beam and the side gate is 130 nm. The measured photodiode current I was converted to a beam center displacement x by using the data in the lower inset. Here, $\partial I / \partial x$ was obtained by scanning the optical spot along the structure. The center of the beam is located at $x = 0$ and the gate at $x = 230$ nm as shown by the shading.

[a)]Author to whom correspondence should be addressed; electronic mail: ekinci@bu.edu

0003-6951/2005/87(11)/113112/3/$22.50

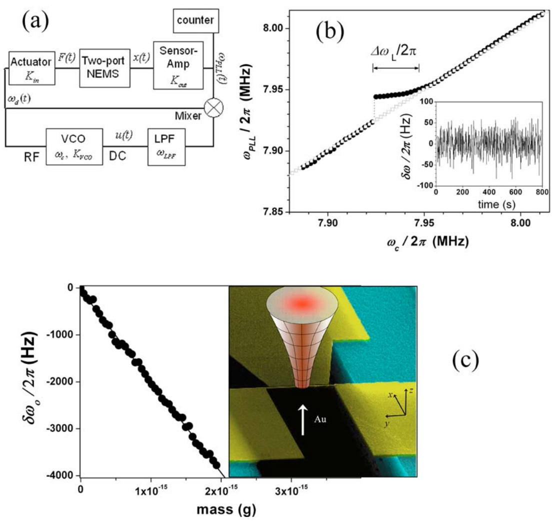

FIG. 2. (Color online) (a) Schematic of the PLL. The NEMS resonator is modeled as a two-port electromechanical device. The following components are used: a voltage controlled oscillator (VCO), a radio frequency (rf) mixer, a low-pass filter (LPF), an amplifier, and a frequency counter. (b) PLL output frequency ω_{PLL} as a function of the VCO carrier frequency ω_c in the vicinity of $\omega_o/2\pi \approx 7.9440$ MHz. Locking is observed for 7.9245 MHz $< \omega_c/2\pi <$ 7.9501 MHz. When the gain of the optical transducer-amplifier cascade is lowered by a factor of 10, frequency locking is no longer present (data in gray). The inset shows the fluctuations in ω_{PLL} while the PLL is locked to ω_o. (c) Resonance frequency shift of the NEMS resonator as thermally evaporated gold atoms are absorbed on its surface. The mass is determined from separate quartz crystal and NEMS surface area measurements. The inset shows the experimental geometry.

resonance measurements, the optical spot was positioned at the point of maximum $\partial I/\partial x$ on the structure, which corresponded roughly to the nanomechanical beam center. Subsequently, the beam was actuated and the photodetector current was monitored. Using this reflection technique, we measured the in-plane fundamental flexural resonances of five beams with dimensions 10 μm$< l <$20 μm, 100 nm$< w <$500 nm, and t=125 nm. The resonance frequencies observed were in the 7 MHz$< \omega_o/2\pi <$20 MHz range.

The block diagram of the PLL is depicted in Fig. 2(a). As the voltage controlled oscillator (VCO), we used a constant amplitude radio frequency (rf) source where the carrier frequency ω_c could be frequency modulated by a quasistatic control voltage $u(t)$. During operation, ω_c was set by the operator; this resulted in a NEMS drive signal at the frequency $\omega_d = \omega_c + K_{\mathrm{VCO}} u$. Here, K_{VCO} is the VCO gain in units of $\mathrm{s}^{-1}\,\mathrm{V}^{-1}$. The optically transduced signal from the NEMS was then mixed with the VCO output and low-pass filtered—to be fed back into the VCO as the control voltage. The low-pass filter bandwidth Δf determined the effective bandwidth of the PLL.

Figure 2(b) demonstrates the operation of the PLL. Here, ω_c was increased by the operator in steps and the frequency of the loop ω_{PLL} was monitored by a frequency counter. For small amplifier gains, no locking was observed (see the data in gray). For larger gains, the PLL locked stably to the resonance frequency at $\omega_o/2\pi \approx 7.9440$ MHz of the beam resonator. The lock range in Fig. 2(b) is 7.9245 MHz$< \omega_c/2\pi <$7.9501 MHz. Note that the lock frequency ω_{PLL} is not exactly equal to ω_o; moreover, it is slightly different for each ω_c. This suggests that there remains a finite but small phase error in the loop.

Within the lock range, the loop stability was monitored as a function of time as shown in the inset of Fig. 2(b). The rms frequency fluctuations $\delta\bar{\omega}$ was $\delta\bar{\omega}/2\pi \approx 51$ Hz for Δf =100 Hz. The observed noise was dominated by the white noise in the amplifier with current noise density $S_I(\omega)$. Using the experimentally determined values $S_I(\omega) \approx 50\ \mathrm{pA}^2/\mathrm{Hz}$, Δf=100 Hz, DR=47 dB,[10] Q=1300, and $\partial I/\partial x \approx 0.7$ A/m, we obtained a reasonable theoretical estimate[2] of $\delta\bar{\omega}/2\pi$ =40 Hz.

TABLE I. Experimentally determined parameters used in the simulations.

Parameter	Value
m	1.4×10^{-15} kg
$\omega_o/2\pi$	7.944×10^{6} Hz
Q	1300
A_d	0.22 V
K_{in}	1×10^{-10} N/V
K_{out}	1.9×10^{10} V/m
K_m	0.1 V^{-1}
K_{VCO}	$6.27\times10^{5}\ \mathrm{s}^{-1}\,\mathrm{V}^{-1}$
$\omega_{\mathrm{LPF}}/2\pi$	100 Hz

In Figure 2(c), we further demonstrate that the PLL tracks the resonance frequency ω_o of the NEMS resonator during mass loading of the resonator. In this set of measurements, mass loading was accomplished by thermally evaporating Au atoms upon the resonator through the back side of the chip [see the inset of Fig. 2(c)]. The Au flux was measured by a quartz crystal. The technique used here is similar to that described in Ref. 2. Fig. 2(c) shows the frequency shift as a function of the added mass; the slope of the plot gives the mass responsivity, $\partial\omega_o/(2\pi)\partial m = -1.95$ Hz/ag (ag $=10^{-18}$ g). This is close to the value -2.15 Hz/ag estimated from the dimensions of the resonator.[2] This corresponds to a minimum detectable mass of $\sim$25 ag, given the above $\delta\bar{\omega}$.

We now turn to the analysis of the PLL operation.[7] A two-port nanomechanical beam resonator—actuated capacitively and transduced optically—is at the center of the PLL. The resonator's displacement $x(t)$ in response to a drive around $\omega \approx \omega_o$ can be determined from the one-dimensional damped oscillator equation as

$$m\ddot{x}(t) + m\frac{\omega_o}{Q}\dot{x}(t) + m\omega_o^2 x(t) = K_{\mathrm{in}} A_d \cos[\theta_d(t)]. \tag{1}$$

Here, m is the effective mass and Q is the quality factor for the fundamental flexural mode. K_{in} is the input transducer responsivity (in units of N/V) and A_d is the constant drive voltage amplitude (in units of V). The phase angle $\theta_d(t)$ of the VCO output signal is defined as

$$\theta_d(t) = \omega_c t + K_{\mathrm{VCO}} \int_0^t u(t')dt'. \tag{2}$$

Note that $\dot{\theta}_d(t) = \omega_d(t)$. The optical transducer-amplifier cascade with responsivity K_{out} (in units of V/m) converts $x(t)$ into an output voltage. This output is mixed with the VCO drive signal and low-pass filtered. This results in

$$\dot{u}(t) = \omega_{\mathrm{LPF}}[K_m K_{\mathrm{out}} x(t) A_d \cos\theta_d(t) - u(t)], \tag{3}$$

where ω_{LPF} is the cut-off frequency of the low-pass filter (LPF) and K_m is the mixer gain (in units of V^{-1}). The output voltage $u(t)$ of the LPF is fed back into the VCO as the control voltage. This set of nonlinear integro-differential

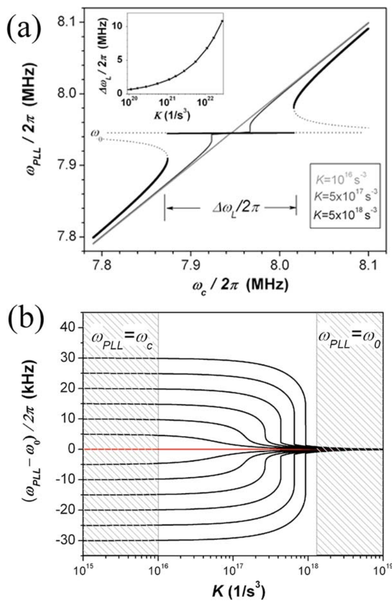

FIG. 3. (Color online) Results from the analysis of PLL operation. (a) ω_c vs ω_{PLL} at different loop gains K. For small K, $\omega_{\mathrm{PLL}}=\omega_c$. Frequency locking is observed beyond a critical gain value $K>K_{\mathrm{cr}}\approx 3\times 10^{17}$ s^{-3}. For these K values, ω_{PLL} is a multivalued function of ω_c. The lock range $\Delta\omega_L$ (inset) increases with increasing K. (b) Frequency flow as a function of K. Locking is observed for $K>K_{\mathrm{cr}}$.

equations given in Eqs. (1)–(3) governs the operation of the PLL.

To gain insight into the PLL operation, we first look at *steady state response*. The starting assumption is that, at steady state, loop response and the VCO control voltage u become time invariant.[11] Consequently, the (transduced) NEMS signal and the VCO output are at the same frequency: $\omega_{\mathrm{PLL}}=\omega_d=\omega_c+K_{\mathrm{VCO}}u$. Using the above relation between the frequencies, setting $\dot{u}=0$, and assuming that the LPF output is at dc, Eqs. (1)–(3) transform into a single algebraic relation between ω_c and ω_{PLL} that describes the steady state,

$$\omega_c = \omega_{\mathrm{PLL}} - K\frac{(\omega_o^2-\omega_{\mathrm{PLL}}^2)}{(\omega_o^2-\omega_{\mathrm{PLL}}^2)^2+\left(\omega_{\mathrm{PLL}}\dfrac{\omega_o}{Q}\right)^2}. \quad (4)$$

Here, K is the total loop gain in units of $1/\mathrm{s}^3$, and $K=K_{\mathrm{VCO}}K_mK_{\mathrm{in}}K_{\mathrm{out}}A_d^2/2m$. The values of the parameters used in our experiments during locked PLL operation [Fig. 2(b)] are listed in Table I. Our experimental K value is 2×10^{18} s^{-3}.

In Figure 3(a), we have plotted ω_{PLL} as a function of ω_c for three different K values using Eq. (4). The function $\omega_{\mathrm{PLL}}=f(\omega_c,K)$ goes through an interesting transformation as K is increased—possibly giving rise to the observed locking behavior. For $K<K_{\mathrm{cr}}\approx 3\times 10^{17}$ s^{-3}, ω_{PLL} is a single-valued function of ω_c, and $\omega_{\mathrm{PLL}}\approx\omega_c$. Thus, frequency locking is *not* observed. For 10^{16} s$^{-3}<K<K_{\mathrm{cr}}$, the inflection points of $f(\omega_c,K)$ around $\omega_c\approx\omega_o$ become more noticeable (not shown), but locking is *still not* present. As K is increased further, ω_{PLL} becomes a multivalued function of ω_c. In Fig. 3(a), we have shown the multivalued nature of $\omega_{\mathrm{PLL}}=f(\omega_c,K)$ by dashed lines, but plotted a single-valued function. Experimentally, these discontinuities correspond to frequency jumps such as those observed in Fig. 2(b). After the jump, locking behavior is observed, i.e., $\omega_{\mathrm{PLL}}\approx\omega_o$. We define the lock range $\Delta\omega_L$ as the frequency interval where $\omega_{\mathrm{PLL}}\approx\omega_o$, regardless of the value of ω_c. In the inset of Fig. 3(a), we display $\Delta\omega_L$ as a function of K. Larger K appears to favor a broader lock range.

Figure 3(b) shows ω_{PLL} as a function of K. In this set of analyses, ω_c is set at a value close to ω_o and ω_{PLL} is determined as K is increased. At low K, ω_{PLL} stays near ω_c. As K is increased, ω_{PLL} is observed to flow towards ω_o. We note that for finite K there remains a small error between ω_{PLL} and ω_o (also observed experimentally). As $K\rightarrow\infty$, the error approaches zero.

The analysis presented here does not capture all aspects of PLL operation. First, the experimentally observed lock range is not symmetric around ω_o [cf. Fig. 2(b) and Fig. 3(a)]. Second, we do not observe hysteresis in ω_{PLL} depending upon the sweep direction of ω_c; such behavior is common[12] in nonlinear systems. We believe that, in going from the dynamic description, i.e., Eqs. (1)–(3), to the steady state approximation, we lose some of the interesting nonlinearities in the system. In an effort to reveal this complex nonlinear behavior, we investigated the numerical time domain solutions of Eqs. (1)–(3).[13] In this analysis (not shown), the expected frequency capture behavior emerged after a period of several milliseconds. However, after long times, we encountered growing truncation errors due to the *stiff* nature of the system.[13] Implicit methods with very small time steps may result in accurate solutions capturing the interesting physics due to the nonlinearities.

We have described the design, operation, and analysis of a PLL to track the fundamental resonance frequency of a NEMS resonator at room temperature. Such NEMS feedback control schemes may find use in timekeeping and sensor applications.

The authors gratefully acknowledge support from the NSF under Grants No. BES-0216274, CMS-0324416, and ECS-0210752. The authors would like to thank Y. T. Yang, X. L. Feng, A. Oberai, and R. Knepper for helpful discussions.

[1]M. L. Roukes, Phys. World **14**, 25 (2001).
[2]K. L. Ekinci, X. M. H. Huang, and M. L. Roukes, Appl. Phys. Lett. **84**, 4469 (2004).
[3]A. N. Cleland and M. L. Roukes, J. Appl. Phys. **92**, 2758 (2002).
[4]K. L. Ekinci, Y. T. Yang, and M. L. Roukes, J. Appl. Phys. **95**, 2682 (2004).
[5]J. R. Vig and A. Ballato, in *Ultrasonic Instruments and Devices*, edited by E. P. Papadakis (Academic, San Diego, CA, 1999), pp. 637–701.
[6]C. T.-C. Nguyen, Proceedings of 2004 IEEE Custom Integrated Circuits Conference, Orlando, Florida, Oct. 3–6, 2004, pp. 257–264 (unpublished).
[7]R. E. Best, *Phase-Locked Loops: Design, Simulation, and Applications*, 4th ed. (McGraw-Hill, New York, 1999).
[8]T. R. Albrecht, P. Grütter, D. Horne, and D. Rugar, J. Appl. Phys. **69**, 668 (1991).
[9]D. W. Carr, S. Evoy, L. Sekaric, H. G. Craighead, and J. M. Parpia, Appl. Phys. Lett. **75**, 920 (1999); T. Kouh, D. Karabacak, D. H. Kim, and K. L. Ekinci, *ibid.* **86**, 013106 (2005).
[10]Nonlinear behavior was observed at a displacement amplitude of $x\approx 20$ nm.
[11]In this approximation, we ignore the small amplitude oscillations sometimes encountered in steady state.
[12]M. Zalalutdinov, K. L. Aubin, M. Pandey, A. T. Zehnder, R. H. Rand, H. G. Craighead, J. M. Parpia, and B. H. Houston, Appl. Phys. Lett. **83**, 3281 (2003); M. C. Cross, A. Zumdieck, R. Lifshitz, and J. L. Rogers, Phys. Rev. Lett. **93**, 224101 (2004).
[13]*Stiff Computation*, edited by R. C. Aiken (Oxford, New York, 1985).